Chemical Physics xxx (2018) xxx–xxx

Contents lists available at ScienceDirect

Chemical Physics

journal homepage: www.elsevier.com/locate/chemphys

A local instantaneous surface method for extracting membrane elastic moduli from simulation: Comparison with other strategies

Christoph Allolio *, Amir Haluts, Daniel Harries *

Institute of Chemistry and the Fritz Haber Research Center, The Hebrew University of Jerusalem, Jerusalem 9190401 Israel

ARTICLE INFO

Article history:
Received 7 December 2017
In final form 4 March 2018
Available online xxxx

Keywords:
Lipid bilayers
Helfrich theory
Curvature elasticity
Tilt modulus
Soft matter
Surface reconstruction
Bending modulus
Surfactants

ABSTRACT

Advances over the past decade have made it possible to extract elastic constants of lipid assemblies from molecular dynamics simulations. We summarize existing strategies for obtaining membrane elastic moduli and clarify the differences in the underlying approaches. We analyze these strategies in depth, including several important advantages and limitations. By addressing these limitations, we obtain a newly formulated spatially local methodology for extracting bending and tilt moduli: The Real Space Instantaneous Surface Method (ReSIS). With its freely available implementation, this method is designed for highly dynamic systems with arbitrary interface geometries. We demonstrate how the method provides consistent results for membranes of arbitrary size. In addition, we describe alternative implementations of various Fourier-space methods, and use these to compare the results from the different available methods and from published computational data. We specifically focus on the tilt modulus, where very large differences between Fourier and real-space based methods are observed, including those derived using ReSIS. These discrepancies are likely due to the known difference between model moduli and thermodynamic moduli that are derived from the corresponding response functions. In addition, we reexamine the issue of angular degeneracy and its effect on conformational ensembles. Finally, a van 't Hoff analysis of the tilt and bending moduli reveals that both modes act as entropic springs and that enthalpy favors nonzero tilt, perhaps heralding the spontaneous lipid chain tilt of the gel phase at lower temperatures.

1. Introduction

The Helfrich functional [1] and its subsequent extensions provide a framework to analyze and predict the shape and fluctuations of lipid membranes and surfactant films in terms of elastic free energy minimization. Modeling the membrane as an elastic, geometric surface or thin sheet gives a simple yet powerful starting point for the interpretation of multiple biophysical phenomena that involve membrane remodeling processes, including endocytocis and fusion [2–9]. Unfortunately, the values for the elastic moduli obtained from experiments scatter over a wide range, so that even for simple one-component membranes there is no single agreed set [10,11]. For a discussion of possible causes see [12]. An additional complication is that real biological cell membranes contain a diverse mix of lipids, cholesterol, and membrane proteins, so that there is very little hope for an experimental consensus on membrane properties for biologically relevant systems in the foreseeable future.

Molecular dynamics (MD) simulations, by contrast, allow the consideration of nearly arbitrary membrane systems, including proteins and ions, on a reasonable timescale and with consistent accuracy [13,14]. Consequently, different strategies to obtain membrane elastic properties from simulation have been developed and proposed in recent years [15–22]. These methods generally fall into two classes: one is based on the equipartition theorem applied to large scale fluctuations via Fourier methods, the other – real space fluctuation method – relies on analyzing localized fluctuations.

With the advance of computational power and methodology it is now possible to regularly compute membrane elastic properties for truly atomistic models. However a similar confusion as in experimental measurements is encountered when applying different methods to extract elastic moduli from MD trajectories. While this may potentially hamper quantitative predictions and comparisons, general trends are usually conserved when a specific method is applied. Here, we compare different established methodologies for extracting membrane properties. We extend the known

* Corresponding authors.
E-mail addresses: allolio@fh.huji.ac.il (C. Allolio), daniel@fh.huji.ac.il (D. Harries).

https://doi.org/10.1016/j.chemphys.2018.03.004
0301-0104/

real-space fluctuations methodology to arbitrary instantaneous surfaces and show its consistency. Finally, we employ this methodology to discuss the origins of the tilt and bending moduli and the differences between methods used to extract it, focusing on the thermodynamic origins of tilt and bend.

2. Fundamentals

The first theory on curvature elasticity of lipid bilayers is the celebrated Helfrich-Canham-Evans theory [1,23,24]. It defines a mechanic (free) energy per surface area as a function of the curvature of an amphiphile monolayer,

$$E = \int d\mathbf{A}\left[\kappa\frac{1}{2}(H - J_s)^2 + \bar{\kappa}K_G\right] \tag{1}$$

where H denotes the monolayer mean curvature, and K_G denotes the monolayer Gaussian curvature, each with an associated modulus, κ and $\bar{\kappa}$. Here and in the following, bold face is used for vector quantities, underlines are used for tensor quantities, superscript indices denote vector components, subscript indices represent derivatives (latin letters) or vector components (greek letters). Exceptions are clearly specified. The mean curvature is defined as

$$H = c_1 + c_2 = \mathrm{Tr}\{\underline{b}\}, \tag{2}$$

where c_1 and c_2 are the principal curvatures and $\underline{b}$ is the curvature tensor; note in passing that the principal curvatures are the eigenvalues of the shape operator **B**. The Gaussian curvature is defined using the same principal curvatures as

$$K_G = c_1 c_2 = \mathrm{Det}\{\underline{b}\} \tag{3}$$

The shape operator **B** of the surface $\mathbf{A}(u, v)$, with surface normals **N** is defined as:

$$\mathbf{B}(v) = -\nabla_v \mathbf{N} = \mathbf{N}_v \tag{4}$$

which yields the curvature tensor

$$\underline{b} = \{\mathbf{N}_u, \mathbf{N}_v\} \tag{5}$$

The spontaneous curvature J_s reflects the tendency of a monolayer to assume a defined *relaxed* curvature. This curvature, around which the energy functional is expanded, results from the opposing forces due to the lipid headgroup size and the size of the hydrophobic moieties (tails). It is thus a lipid-composition specific property.

Ben-Shaul and coworkers have shown that the elastic moduli of the Helfrich theory can be extracted based on mean field molecular theory [25,26]. However, in some cases lipid membranes can take up ripple or gel phases, or even assume other forms or phases, which are generally not amenable to the standard Helfrich theory [27]. To treat these complex interfaces, additional terms were introduced into the Hamiltonian, whose role is to account for the lipid microscopic structure and degrees of freedom in a simplified way. In the spirit of the Frank theory of liquid crystals [28], it is possible to introduce a director vector **n**, which describes the orientation of the lipid, pointing from the lipid's head to its tails. This modification allows to treat strong local deformations, such as encountered in the membrane fusion stalk [29]. The deviation of the director with respect to the surface normal **N** is defined as the tilt vector **t**:

$$\mathbf{t} = \frac{\mathbf{n}}{\mathbf{n}\cdot\mathbf{N}} - \mathbf{N} \tag{6}$$

This vector is always tangent to the membrane plane. Up to second order, this relation can be approximated as

$$\mathbf{t} \approx \mathbf{n} - \mathbf{N} \tag{7}$$

The Hamiltonian is then extended to become the Kozlov-Hamm [30]-Helfrich (KHH) functional:

$$E = \int d\mathbf{A}\left[\kappa\frac{1}{2}(\widetilde{H} - J_s)^2 + \frac{1}{2}\kappa_\theta \mathbf{t}^2 + \bar{\kappa}\widetilde{K}_G\right] \tag{8}$$

The curvatures H, K_G have been modified to be functions of the director **n** instead of the normal vector **N** and furthermore a tilt modulus κ_θ arises to describe the cost of perturbing the alignment of **n** with the membrane normal. The *effective* curvature can then written as

$$\widetilde{H} = -\mathrm{Div}(\mathbf{n}) = H - \mathrm{Div}(\mathbf{t}) \tag{9}$$

The implication of this is that the bending deformation is equivalent to a tilt deformation in the plane, an assumption which bears close resemblance to the *pyramid approximation* of Szleifer et. al. in their chain packing theory [25,26]. Note, however, that the divergences given in the last equation are covariant divergences. When written explicitly they take the form

$$\mathrm{Div}(\mathbf{n}) = \frac{dn^u}{du} - \Gamma^u_{wu} n^w + \frac{dn^v}{dv} - \Gamma^v_{wv} n^w \tag{10}$$

where u, v are the parametrization variables of the surface, Γ are Christoffel symbols of the second kind and the Einstein summation convention implies a sum over the index w. The differentiation of **n** has to be taken at the membrane dividing surface (see below). Therefore, this approach also requires knowledge of the surface and its fundamental forms, at least in principle.

3. Strategies

The basic strategies for obtaining elastic moduli are either based on real-space or on Fourier-space analysis. Both methods rely on the equipartition theorem, but use a different set of approximations. Thus, extraction of bending rigidities and other elastic moduli requires the analysis of the fluctuations of an equilibrated system. Typically, such fluctuations are sampled from an (on average) flat bilayer, with an aqueous interface, under periodic boundary conditions. Periodic boundary conditions are essential for minimizing artifacts, but render simulations of unsupported monolayers very difficult. Most strategies therefore focus on the analysis of simulated bilayers. In the following, we briefly review these methodologies and outline the basic assumptions and approximations associated with each approach.

3.1. Fourier methods

3.1.1. Height fluctuation method

The Fourier space analysis methods are older, with the most basic one relying on the unmodified Helfrich functional [31]. Usually, only a flat periodic bilayer is considered. A Monge patch in the canonical basis is used to describe the surface $\mathbf{S}(x, y) = [x, y, f(x, y)]^T$. The curvature is considered to be relatively small and is linearized to give

$$H \approx \frac{d^2 f}{dx^2} + \frac{d^2 f}{dy^2} \tag{11}$$

Due to the Gauss-Bonnet theorem, any energy contribution from the term containing K_G can be excluded, as it remains constant as long as topology is maintained. The system analyzed is a periodic bilayer that is on average flat. Therefore any height fluctuation is considered to be due to a bilayer fluctuation. The spontaneous curvatures of the upper and lower leaflet of the lipid bilayers cancel, so that the bilayer spontaneous curvature J_s^b is zero within the linearization. The Helfrich (free) energy thus becomes

$$E^b = \frac{1}{2}\int\int \kappa^b\left[\frac{d^2 f}{dx^2} + \frac{d^2 f}{dy^2}\right] dxdy \tag{12}$$

Please cite this article in press as: C. Allolio et al., Chem. Phys. (2018), https://doi.org/10.1016/j.chemphys.2018.03.004

where we have inserted the superscript b to denote that the energy and bending modulus are bilayer quantities. Bilayer and monolayer quantities are closely related and it is easy to see that as long as membrane thickness is neglected, $\kappa^b = 2\kappa$, where κ is the monolayer modulus.

Next, the height function is expanded in a Fourier series:

$$f = \frac{1}{A}\sum_k\sum_j \tilde{f}(k,j)\exp[i\pi(kx+jy)] \tag{13}$$

We define a vector $\mathbf{q} = [k,j]^T$, integrate, and find the energy to be the sum of independent contributions,

$$E^b = \frac{1}{2}\sum_k\sum_j \kappa^b||\mathbf{q}||^4|\tilde{f}(\mathbf{q})|^2 \tag{14}$$

Because the energy of each degree of freedom should be $k_BT/2$, the value of the summands $|\tilde{f}|^2$ as a function of the Fourier-space vector $\mathbf{q}$ scales as

$$\langle|\tilde{f}(\mathbf{q})|^2\rangle = \frac{1}{\kappa^b||\mathbf{q}||^4} \tag{15}$$

The bilayer bending modulus emerges when $|\tilde{f}|^2$ is plotted against $||\mathbf{q}||^4$, which reaches a plateau for low $||q||$, see also Fig. 1. In practice, the mean values of $|\tilde{f}|$ are obtained by Fourier-transforming the z-positions of a set of lipid atoms on a grid.

3.1.2. Director fluctuation method (DF)

This method is due to Watson and Brown [15], building on earlier work by Kopelevich et al. [20]. It uses director fluctuations from an extended KHH Hamiltonian to extract the moduli. To summarize the main approach: as a first step, a bilayer director vector is defined

$$\mathbf{n}^b = \frac{1}{2}[\mathbf{n}^{up} - \mathbf{n}^{down}] \tag{16}$$

where each $\mathbf{n}^b = [n^x, n^y]^T$ is a 2D-vector. The averaging over upper and lower leaflets is performed in order to decouple from peristaltic modes (which can be sampled, by using the + sign in the linear combination). We note that if we take the view of an average surface in the xy plane, this vector is equal to the tilt vector $\mathbf{t}^b$ within the approximation of Eq. (7).

The part of the Hamiltonian that is relevant for computing the bending energy is

$$E_\kappa = \int\int \kappa^b\left[\frac{d\mathbf{n}^b}{dx} + \frac{d\mathbf{n}^b}{dy}\right]dx\,dy \tag{17}$$

We note that the implicit assumption with respect to Eq. (10) is that the explicit dependence on the surface is neglected so that the xy plane is considered to be approximately a tangent to the surface at all times. If this is no longer the case, as e.g. in Fig. 2, tilt deformations are not sampled properly. The actual tilt contribution is mixed with a twist contribution with modulus κ_{tw}, so that:

$$E_{\kappa_\theta} = \frac{1}{2}\int\int\left[\kappa^b_\theta(\mathbf{t}^b)^2 + \kappa^b_{tw}\nabla\times\mathbf{t}^b\right]dx\,dy \tag{18}$$

The equations are transformed to Fourier space in the same way as described in the height fluctuation method. Then, a Helmholtz decomposition is introduced to separate the director field into a rotation-free part $\tilde{n}_\parallel = \frac{1}{q}[\tilde{\mathbf{n}}\cdot\mathbf{q}]$ and divergence free-part $\tilde{n}_\perp = \frac{1}{q}[\tilde{\mathbf{n}}\times\mathbf{q}]\cdot\mathbf{e}_z = \tilde{m}_\perp$. This allows to separate contributions of twist from the bending deformations. The equipartition theorem then yields

$$\langle|\tilde{n}(\mathbf{q})_\parallel|^2\rangle = \frac{1}{\kappa^b||\mathbf{q}||^2} \tag{19}$$

and

$$\langle|\tilde{n}(\mathbf{q})_\perp|^2\rangle = \frac{1}{\kappa^b_\theta + \kappa^b_{tw}||\mathbf{q}||^2} \tag{20}$$

Instead of Fourier coefficients of height, projected director Fourier contributions are collected. This method usually converges relatively quickly with patch size (i.e., at relatively high $\mathbf{q}$) due to its use of the highly localized tilt fluctuations (compare Fig. 1, left). In Fig. 1 right panel, we show the fit of Eq. 20 applied to a example of a 1024 lipid per leaflet MARTINI [32,33] coarse-grained force field patch. The reciprocal-parabolic fit usually loses validity at $q \geqslant 2\ \mathrm{nm}^{-1}$.

3.1.3. Limitations and new approaches

The methods outlined to this point have been demonstrated to be empirically and theoretically sound [34,35,15]. However, they are subject to binning errors and Fourier uncertainty or truncation artifacts. They also typically require relatively large lipid patches to converge, so that enough lipids are available to populate sufficiently each grid point. In our experience, these restrictions translate to a lower bound of about 400 lipids per leaflet for the tilt fluctuations method and around 1000 lipids per leaflet for the height fluctuation method. In Fig. 1 left panel, we show the different convergence behavior of the Fourier methods on a membrane patch containing 1024 MARTINI force field lipids, per leaflet.

Rather than proposing to change these methods, we instead suggest to reduce noise and locality by using a different binning strategy, as described below in the Implementation Details section of the Supporting Information (SI). Another limitation is the restriction to flat periodic lipid patches. While almost all published simulations are of this type, large scale deformations are perhaps the most interesting systems to be described by the Helfrich theory. Both local modification and large scale deformations, such as protrusions, escape these methods. In principle, it is possible to adapt the method, for example to vesicles, by changing the (local) coordinate system. However, in the general case this requires solving the continuum shape equation first, and then monitoring fluctuations for each system [36]. This approach is hardly generalizable and would require careful attention to each new simulation type.

3.2. Local methods

We have previously proposed the real-space fluctuation methodology [18,16] that analyzes the fluctuations of lipids locally. This strategy relies on several assumptions. The first is that the moduli can be extracted from local, rather short-ranged, fluctuations on the molecular scale. This is plausible because the tilt vector is known for decades to act as a localized molecular property. Indeed, mean field theories based on single molecule (or even single-chain) analysis succeed in accurately predicting the elastic moduli [25,37]. In the top panel of Fig. 2 we schematically illustrate how the pyramid approximation would give rise to the same modulus for tilt and normal vector divergence. We also give two schematic examples on how an instantaneous bilayer deformation can be either associated purely with lipid splay, or with lipid tilt.

3.2.1. Real Space Gibbs Dividing Surface Method (ReGiS)

The REGiS method is a variant of the real-space approach that aims to compute the elastic moduli of the lipids using local sampling on an averaged surface. We will now restate this method, clarifying some misconceptions on the nature of the calculated quantities. The ReGiS method originally used the lipid tilt and lipid

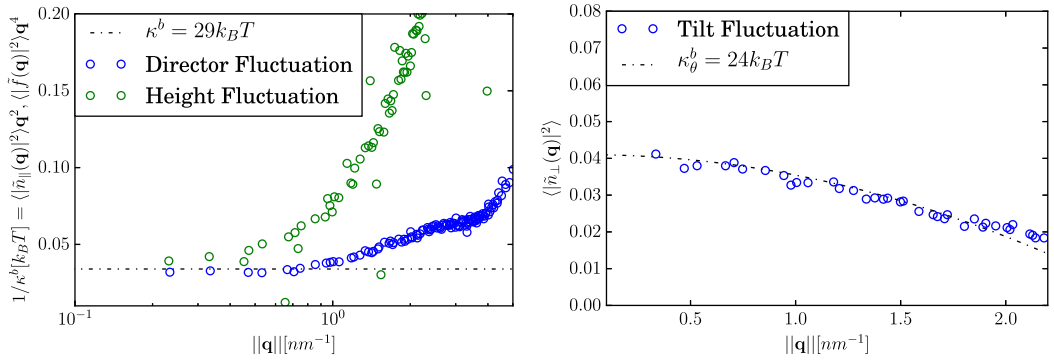

Fig. 1. Left panel: Bending modulus determination from height fluctuation and director fluctuation analysis in Fourier space performed on a 2048 lipid DOPC patch (coarse-grained simulation, see details in the SI). Right panel: Tilt modulus determination from Fourier space fluctuations.

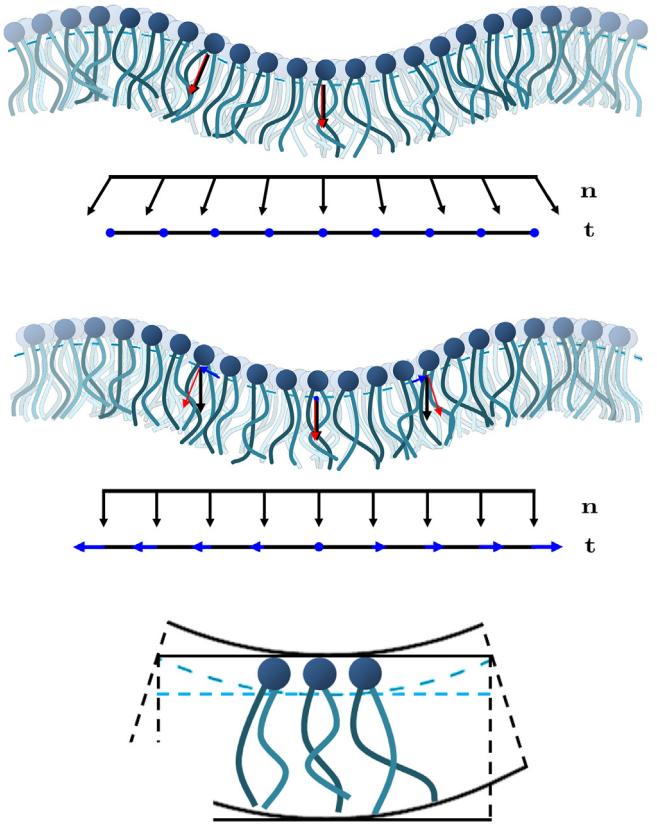

Fig. 2. Top panel: Scheme of the pyramid approximation, Bottom panels: Schematic drawing of tilted and untilted monolayer bending deformations with the same interface. Director vectors are drawn in black, tilt vectors in blue, and membrane normals in red. The dashed line represents the dividing surface. (For interpretation of the references to colour in this figure legend, the reader is referred to the web version of this article.)

splays as its central quantities. The splay was initially estimated by an angle between two lipids, which could be thought of as an approximation of the covariant divergence of the lipid director Div(**n**). Recently, the method was reformulated in terms of the (covariant) derivative of the director vector and generalized to arbitrary stable lipid interfaces [16,38]. In this method, both the director vector **n** and the surface normal **N** are explicitly calculated. To obtain the surface, solvent and lipid densities are computed and smoothed. The trajectory is then aligned with a reference frame by minimizing overlaps of lipid and water densities as well as maximizing overlap with the density map of the same component [38]. The surface normals **N** are taken at the Gibbs interface, as determined by the density of water molecules at the aligned lipid interface.

The lipid splay S is then calculated as

$$S = \lim_{h\to 0} \frac{n^\alpha(\alpha_0 + h^\alpha) - n^\alpha(\alpha_0) - (N^\alpha(\alpha_0 + h^\alpha) - N^\alpha(\alpha_0))}{||\mathbf{h}||} \tag{21}$$

This is done by directly using a local, approximate, tangent plane in an orthonormal basis $\mathbf{A}(\alpha, \beta)$, noting that upper indices mark the components of the vector in this basis. The basis is formed around the lipid position (α_0, β_0). As the tangent vector $\mathbf{A}_\alpha$ is chosen to point in the direction of the neighboring lipid, changes along e^β are minimal. However, the limit $h \to 0$ is in practice never reached (as lipids are mutually excluded and cannot become arbitarily close) but rather **h** is the distance between two lipids. When we write the splay as

$$S \approx \nabla_h[\mathbf{n}] - \nabla_h[\mathbf{N}] \approx \mathrm{Div}(\mathbf{t}) \tag{22}$$

(the ∇_h here denote forward finite differences), and compare to Eq. (7) we can immediately realize that this is an approximation of Div(**t**), not of Div(**n**). However, only one component of Div(**t**) is calculated – the orthogonal $\mathbf{A}_\beta$ is neglected. Johner et al. showed, that this estimator is uncorrelated beyond two neighboring lipids [16]. The metric corrections for the covariant derivative are also neglected. Furthermore, it is generally postulated that $\langle \mathrm{Div}(\mathbf{t})\rangle = 0$, i.e. that there is no average tilt in the liquid phase [30].

The energy contribution per lipid from the tilt divergence is

$$E^l_{\mathrm{Div}(\mathbf{t})} = \frac{1}{2}\kappa[\mathrm{Div}(t)]^2 A_l \tag{23}$$

The probability distribution should therefore be

$$P(S) \propto \exp\left[-\frac{1}{2}\kappa\beta S^2 A_l\right] \tag{24}$$

with $\beta = 1/k_BT$ and A_l the area per lipid. Then we can extract κ by taking the logarithm and fitting the distribution to a quadratic expression:

$$\log P(S) = -\frac{A_l\kappa}{2}S^2 + C \tag{25}$$

with κ given here in units of k_BT. An equivalent approach can be taken with the tilt modulus κ_θ. Bending moduli obtained with this method have been carefully validated and reported in a number of papers [11,18,16].

The lipid tilt is a molecular quantity, defined using the director by Eq. (6) and usually approximated by Eq. (7). Because by definition it is a molecular quantity, and is additive in the KHH Hamiltonian, the per-lipid contribution is

$$E_t^l = \frac{1}{2}\kappa_\theta \mathbf{t}^2 A_l \tag{26}$$

where A_l is the area per lipid. In the early ReGiS approach, the tilt vector was approximated by the angle θ, between director $\mathbf{n}$ and the surface. For the angle θ, a cone degeneracy correction of sin θ is generally applied. Therefore, we can use

$$P(t) \propto (\sin\theta)^{-1} \exp\left[-\frac{1}{2}\kappa_\theta \beta \theta^2 A_l\right] \tag{27}$$

to fit the tilt modulus to the potential of mean force (PMF) obtained from simulations.

3.2.2. Limitations of the method

The REGiS method has a number of potential drawbacks and conceptual inconsistencies. To understand the problem it is instructive to look at the lower part of Fig. 2. The heart of the problem is the conflict of average and instantaneous surfaces. We know from Eq. (14) that membrane height fluctuations scale with q^{-4}. This means that increasingly large bilayers will result in very large membrane fluctuations. Using an average surface does not account for this scaling behavior. A fairly strong, yet temporary deformation, as depicted in Fig. 2, will therefore be captured inaccurately. This is because, as seen from the average surface, the bending deformation of the upper panel is picked up as a tilt deformation. This is not necessarily a problem for the splay, i.e. for deriving the bending modulus, because a tilt gradient contributes in the same way as a true splay deformation. Nevertheless, this becomes problematic especially in the case of the ReGiS implementation, because surface deformations are often nonlocal, violating the basic locality assumption of the method. Furthermore, the described misidentification can be expected to lower the tilt modulus, because an apparent, nonexisting tilt is sampled. On the other hand, the ideal or "pure" tilt deformation shown in the lower panel of Fig. 2 would not be picked up, as all director vectors are aligned with the average interface. While such a deformation will rarely be observed, it still demonstrates the problem encountered in identifying the correct deformation mode. We note, that this problem also exists and is relevant in the director fluctuation method as originally derived and currently implemented.

It is, therefore, necessary to compute the tilt on an instantaneous surface. This requires a fast and accurate method for obtaining such a surface. In the discussion of the height fluctuation method, we have pointed out the difficulty of such an approach: the instantaneous surface truly behaves as a surface only on rather large length scales. The roughness encountered on short scales has been realized for a long time, and is often ascribed to protrusions, i.e. lipids sticking in and out of the interface [31,39]. Beyond the fundamental issues, the calculation of the Gibbs interface in the ReGiS method is computationally demanding and requires alignment of the trajectory. Thus, an instantaneous surface of sufficient quality would also be beneficial for speeding up calculations.

3.2.3. Real Space Instantaneous Surface Method (ReSIS)

To construct the instantaneous surface, we employ here a local least-squares fitting approach to an extended lipid environment (see Implementation Details in the SI). The instantaneous surface also allows us to introduce a different approach towards obtaining κ, based on a fully instantaneous estimate of Div($\mathbf{t}$). To obtain the decoupled (and therefore local) tilt deformation, we take a look at the composition of the full instantaneous curvature matrix:

$$\underline{\tilde{b}} := \tilde{b}_\alpha^\beta = b_\alpha^\beta - t_\alpha^\beta \tag{28}$$

The greek indices refer to the variables of the surface parametrization. While the curvature tensor $\underline{b}$ can be computed from the surface, we need only compute the tilt tensor to obtain the bending modulus κ, because the tilt divergence has the same modulus as the bending of the whole membrane. The components of the tilt tensor are given by

$$t_\alpha^\beta = \frac{\partial t^\beta}{\partial \xi^\alpha} + \Gamma_{\alpha\nu}^\beta t^\nu \tag{29}$$

Here The Christoffel symbols Γ refer to the metric of the membrane surface and ξ denotes vectors of a local tangent basis of the instantaneous membrane. It is worth pointing out again that the tilt vector components t^β need to be computed on this instantaneous membrane surface as well, otherwise the definition of tilt is inconsistent between tilt and bending modes. As in the ReGiS method, we need an estimator for Div($\mathbf{t}$) = Tr$\underline{t}$. For a full evaluation of t_α^β, a locally twice-differentiable instantaneous surface is required, whereas $\mathbf{t}$ should be differentiable at least once. A typical output of this method is given on the left panel in Fig. 3. The distribution is Gaussian and very similar to the ReGiS output [38]. The metric deformations tracked by the Christoffel symbols are typically neglected. Although we too find their contribution to be minimal, they remain in the implementation in view of possible future applications to systems with strong Gaussian curvature.

3.2.4. Tilt modulus and tilt vector degeneracy

The tilt vector computed on the instantaneous surface according to Eq. (6) may be expected to yield a Gaussian-shaped PMF just like the tilt divergence. If the square of the mean tilt satisfies $\langle\mathbf{t}\rangle^2 = 0$, the tilt modulus can be calculated from the variance of $\mathbf{t}$ of single lipids according to Kozlov et al. [37]:

$$\langle\mathbf{t}^2\rangle \frac{A_l}{k_B T} = \frac{1}{\kappa_\theta} = \chi \tag{30}$$

where χ is the thermodynamic susceptibility with respect to the tilt deformation. However, as we have already seen in the discussion of the ReGiS method, a degeneracy exists. As long as no approximations are made, tilt is a 2D-vector in the local tangent basis. We find (as can be seen in Fig. 4), that the components of this vector t_α in the local orthonormal tangent basis $\{\mathbf{e}_x, \mathbf{e}_y\}$ are uncorrelated, so that the probability density factorizes as follows

$$\begin{aligned} P(\mathbf{t}) &= P(t_x, t_y) \to P(t_x)P(t_y) \\ &= \frac{\sigma}{\sqrt{2\pi}} \exp\left[-\frac{t_x^2}{2\sigma^2}\right] \frac{\sigma}{\sqrt{2\pi}} \exp\left[-\frac{t_y^2}{2\sigma^2}\right] \end{aligned} \tag{31}$$

The variance of the tilt is then

$$\langle\mathbf{t}^2\rangle = \int_{-\infty}^{\infty}\int_{-\infty}^{\infty} dt_x dt_y P(\mathbf{t})\mathbf{t}^2 = \langle t_x^2\rangle + \langle t_y^2\rangle = 2\sigma^2 \tag{32}$$

This expression shows that $\langle\mathbf{t}\rangle^2 = \langle t_x\rangle^2 + \langle t_y\rangle^2 = 0$. Using the polar coordinate transform

$$\langle\mathbf{t}^2\rangle = \int_0^\infty t \frac{1}{\sigma^2} \exp\left[-\frac{t^2}{2\sigma^2}\right] t^2 dt = \int_0^\infty P(t) t^2 dt \tag{33}$$

makes it possible to save the 2D integration and use local fitting in the vein of Eq. (24). For this purpose, the distribution $P(t)$ should be divided by $t = ||\mathbf{t}||$. The variance σ^2 of the resulting Gaussian is half the variance of the full distribution in Eq. (32), and hence the resulting modulus has to be divided by two. We also note that the approximation

$$(\mathbf{n} - \mathbf{N})^2 = \mathrm{crd}^2\theta = 4\sin^2(\theta/2) \approx \theta^2 \tag{34}$$

is valid up to second order. The chord function, crd, describes the distance between two points on the unit circle, separated by the angle θ at the center. We therefore use Eq. 27 as in the ReGiS method. Alternatively, one may also use the full tilt, which will

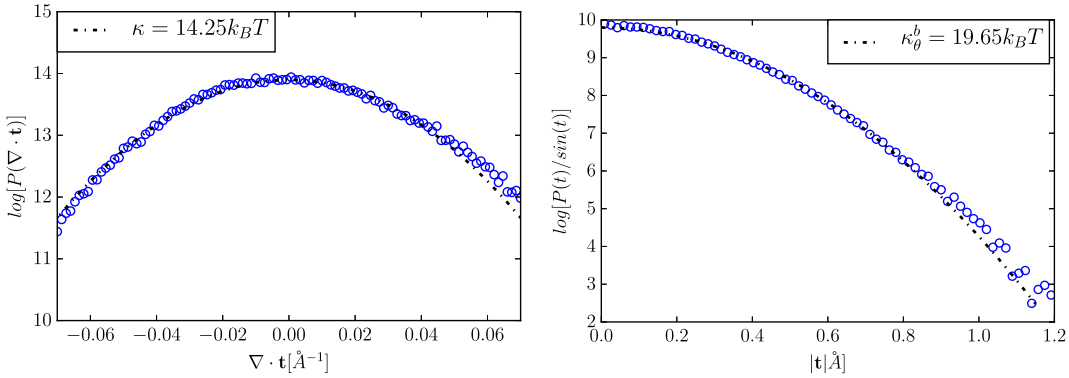

Fig. 3. Left panel: Bending modulus determination by ReSIS from analyzing the PMF for an example of an all-atom POPC patch, Right panel: Tilt modulus determination using the same method and lipid patch. Simulation details can be found in the SI.

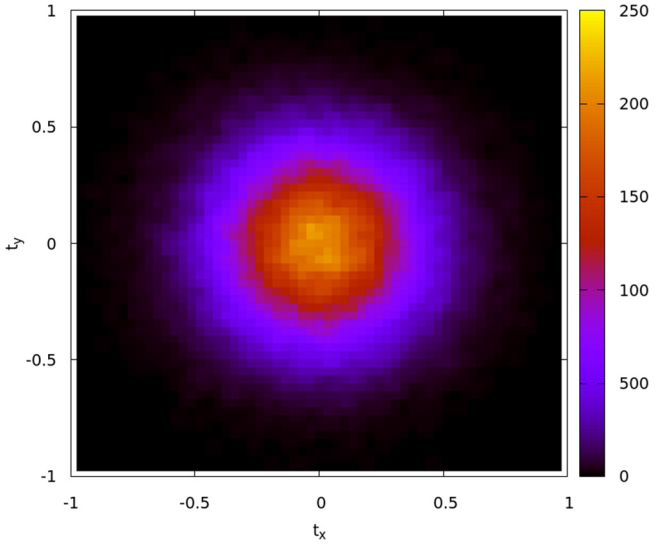

Fig. 4. Tilt components probabilities in two dimensions for the example of POPC. Tilt vectors are dimensionless. The color scale is proportional to the probability density. (For interpretation of the references to colour in this figure legend, the reader is referred to the web version of this article.)

yield $\mathbf{t}^2 = \tan^2\theta$. Again, a quadratic equation is fitted, as in Eq. (25). When using the variance obtained from this equation, e.g. with Eq. (24), such as implemented in [38], $\kappa_\theta^b = 2\kappa_\theta$, i.e. a bilayer tilt modulus is obtained. Because the tilt is unitless, its modulus is obtained in units of k_BT nm^{-2}.

We note that we have included the degeneracy into the susceptibility mostly to allow comparison with the director fluctuation method. In this method the degeneracy of the tilt is not taken into account, as its contribution to the energy would otherwise have to be k_BT and not $\frac{1}{2}k_BT$. In the case of anisotropic tilt deformations, as may be encountered in biological membrane systems, the degeneracy may well be lifted, necessitating a component-wise (anisotropic) tilt modulus. Whether this case is encountered can directly be read from the shape of the 1D tilt distribution.

3.2.5. Pressure tensor

Another established way to extract elastic properties of membranes is through the calculation of lateral pressures. We will not review this methodology in detail, but for completeness we outline its basic concept. This method was derived in the context of the KHH and Helfrich continuum theories [1,30] and has been put on a molecular basis by Szleifer et al. [25]. In the molecular theory, the lateral (say monolayer) pressure π arises as a Lagrange multiplier in the minimization of the free energy of the bilayer. This Lagrange multiplier represents the packing constraint of the lipid chains, as well as surface tension contributions. Relations between the elastic constants and lateral pressure can be obtained, so that

$$\kappa J_s = \int_0^l (z-d)\pi(z)dz \tag{35}$$

Using this approach, the Gaussian bending modulus can also be derived using

$$\bar{\kappa} = -\int_0^l (z-d)^2\pi(z)dz \tag{36}$$

The integration is carried out along the membrane normal z from the bilayer midplane at 0 to the end of the interface at l. Here d is the position of the neutral plane. While these equations do not yield κ directly, this modulus can be obtained together with J_s in combination with one of the other methods. Although attractive as a methodology, the principal technical difficulties with this method are the decomposition of the virial, which is ambiguous in the case of many body potentials, and the localization of the Coulomb interactions. A current implementation and discussion [40] can be found online.[1] Noteably, when using this method, it should always be verified that the normal pressure corresponds to the pressure given by the barostat; discrepancies in this values suggest one of the discussed numerical pathologies.

4. Fundamental differences between methods and formulations

4.1. Locality

An important advantage of the real space methods with respect to the Fourier-space methods is their locality. This locality is a highly desirable property, because it allows us to decompose and spatially dissect the influence of large macromolecular adsorbents or inclusions, as well as other perturbations to the membrane. This renders the method incredibly valuable for the analysis of biologically relevant systems. To demonstrate again the validity of this approach, we compute the spatial correlation function of the tilt for a simulated membrane patch. Results are shown in Fig. 5. While the tilt fluctuations are not entirely uncorrelated, the correlation length is close to the average lipid-lipid distance, so that it is short enough to allow us to ignore correlations within our analysis.

[1] http://www.lacan.upc.edu/LocalStressFromMD.

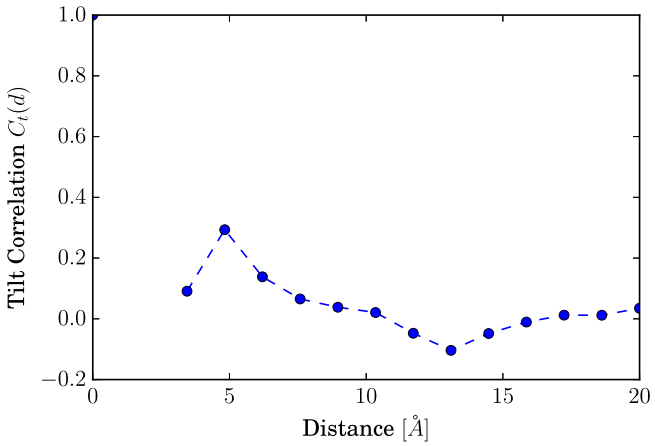

Fig. 5. Spatial correlation function of lipid tilts versus distance between lipids, analyzed for an all-atom POPC membrane trajectory. Lines are intended as a guide for the eye. For simulation details see the SI.

4.2. The surface

When parametrizing continuum models from atomistic simulations, it is notoriously difficult to define the continuum limit. Surfaces are especially hard to get right, as is evidenced by the large volume of literature devoted to surface reconstruction, reviewed, e.g., in [41]. As a validation of our approach, we now aim to check how insensitive the ReSIS method is to the size of the simulated membrane patch. Letting the size of the membrane go to infinity, the population of low q values in the height profile will become very large, reflecting strong deformations. We therefore expect an increasing difference between the instantaneous and average surfaces, as used in ReSIS versus ReGiS, respectively. Importantly, we can expect a change with membrane size in the moduli obtained when using ReGiS, while results from ReSIS should remain insensitive to patch size. In Fig. 6 we show the dependence of obtained tilt and bending moduli on system size. We find that when using the average-surface ReGiS method, the tilt modulus decreases with increasing patch size. In contrast, the predictions from ReSIS are insensitive to membrane patch size up to 4096 lipids per leaflet. We, therefore, recommend using ReSIS for the computation of tilt moduli, particularly in large systems of over 1000 lipids per leaflet. In the left panel of Fig. 6 we compute the bending modulus κ using our tilt interpolation scheme, but assuming constant normal vectors, close to the scheme employed in ReGiS. The bending modulus is almost unaffected by reference surface fluctuations up to a system size of 4096 lipids per leaflet. However, we find consistently lower bending moduli obtained when using the constant, flat surface as compared with the instantaneous surface. This difference is likely due to the contribution of the instantaneous deformation in the short range. The differences between moduli are smaller than those found when using the Fourier-space director fluctuation method, represented by the dashed lines in the plot, but the trend is well represented. Note also, that the original ReGiS bending moduli in this case are lower, with the DOPE value being $\kappa = 10\ k_BT$ [16].

4.3. Multi-component lipid membranes

In earlier implementations [18] we have used an empirical mixing rule for multi-component lipid patches, based on the assumption of coupled harmonic oscillators. This was required because the splay in that implementation was computed only between neighboring lipid pairs and therefore an interaction was always computed per pair type. More generally, studies have usually refrained from applying Fourier methods to lipid mixtures. However, baring large-scale demixing and insufficient sampling, there is no a priori reason to do so, and in the results section we give some examples where the real space and Fourier space methods were implemented to mixtures. Directly computing the divergence of the tilt field locally, or using properly sampled Fourier methods allows us to test the validity of the proposed mixing rule. As can be seen from Fig. 7, the mixing rule generally yields similar results to those computed from the divergence of the tilt field. We, therefore, consider both approaches equally valid. The mixing rule has the distinct advantage that per-pair bending moduli are obtained. Although these are not currently experimentally observable quantities, deriving their values may yield additional physical insight.

4.4. Thermodynamic versus model quantities

The real-space approaches and the Fourier-space approaches are designed to extract somewhat different moduli. While the real space methods treat the moduli as *thermodynamic* parameters (related to a free energy expansion) or as inverse generalized susceptibilities [37], the Fourier based methods extract *model* or Hamiltonian parameters [12]. While the difference between the two approaches and parameters has previously been discussed, and relations between them have been derived under certain assumptions [37,12], to appreciate the difference between these two parameters it may be useful to use a more familiar analogy. Consider an Ising model for spins in the absence of field, and Hamiltonian

$$\mathscr{H}_I = -J\sum_{ij} S_i S_j \tag{37}$$

The magnetization $m_I = S_i$ could be regarded as the analogue of the average tilt. The related magnetic susceptibility is the analogue of the tilt susceptibility, which is just the inverse of the tilt modulus [37]. In the mean field approximation, the Ising susceptibility is

$$\chi_I = \frac{1}{k_BT - zJ} \tag{38}$$

where z is the lattice coordination number [42]. The relation between the Hamiltonian interaction parameter, J, and the thermodynamic one, $k_BT - zJ$, becomes apparent. Specifically, a term related to an entropic contribution arises naturally, separating the values of the two constants. In the spirit of Landau theory, the free energy of the fluctuating Ising system $g(T)$ can be now expanded in terms of the order parameter m_I, so that

$$g(T) = a(T) + \frac{b(T)}{2} m_I^2 + \ldots \tag{39}$$

where at the mean field level, $b(T) \sim T - (zJ/k_B)$ becomes the analogue of the thermodynamic tilt modulus, and is clearly distinct from the model interaction parameter J.

The difference between the two moduli has sometimes been obscured in the lipid elasticity literature, leading to some confusion, since both are generally referred to simply as the tilt modulus κ_0. This ambiguity of nomenclature masks the difference between thermodynamic and model moduli: although thermodynamic and model moduli are intimately related, they are not identical. How they are related will sensitively depend on the details of the specific system and its degeneracies. Just as for the Ising model, the real space tilt and bending moduli are extracted by expressing the free energy in terms of an order parameter (say tilt [43]) and finding the relevant prefactors using the fluctuation-dissipation relations. The physical interpretation of the thermodynamic moduli are similar too: they are related to the expected response to an elastic deformation of the lipids, and can be directly used to calculate the free energy penalties for such deformations. Although this

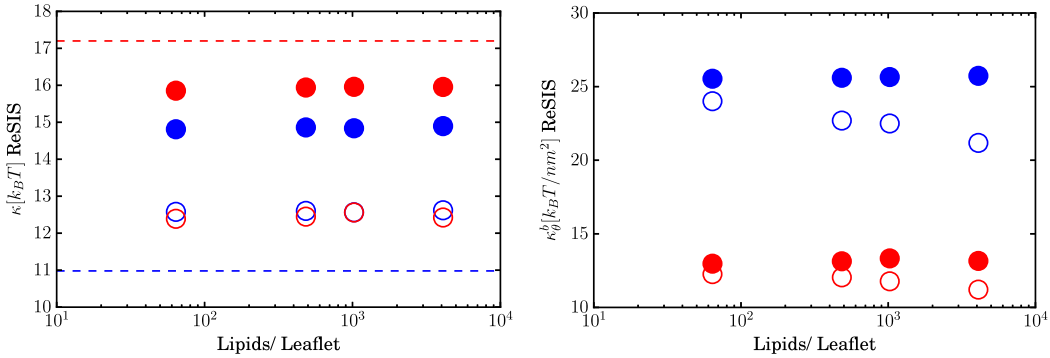

Fig. 6. Scaling of results from the ReGiS (non-instantaneous surfaces) and ReSIS (instantaneous surface) with membrane patch size. Left panel: Bending modulus, Right panel: Tilt modulus. In both panels filled circles are used for ReSIS and empty circles for average surface calculations. Red represents DPPC, blue represents DOPE. In the left panel the DF result is given with a dotted line. In the right panel, for visualization purposes κ_θ^b of DPPC is shifted down by 10 k_BT. For simulation details see the SI. (For interpretation of the references to colour in this figure legend, the reader is referred to the web version of this article.)

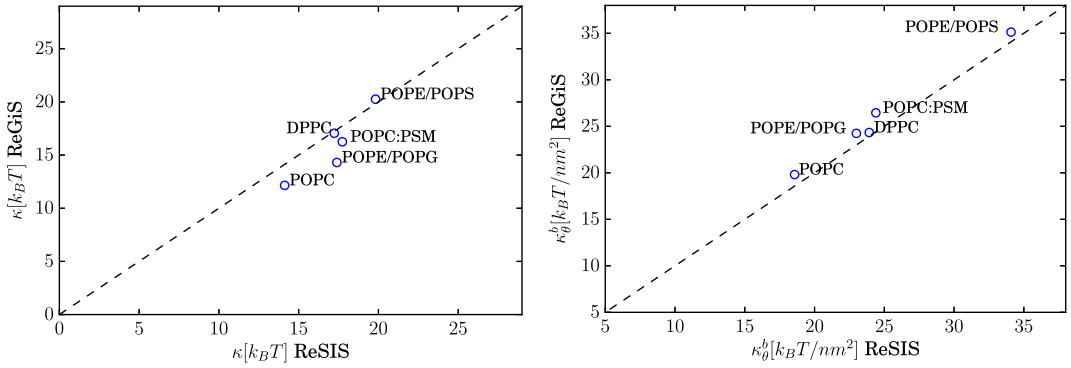

Fig. 7. Comparison of moduli derived from ReSIS and ReGiS for the same lipid trajectories, with REGiS data taken from [11]. Left panel: Comparison of monolayer bending moduli, Right panel: Comparision of bilayer tilt moduli. For simulation details see the SI and [11].

analogy may be helpful to underscore the distinct definition for model and thermodynamic moduli, it is important to note that in the simple Ising model, J is temperature independent, while for the model moduli this is not generally true. This can result in differences in the expected temperature dependence of the moduli, as we further discuss in the Results below.

5. Results

5.1. Systems simulated

We simulated a number of lipid patches using the MARTINI force field, each of different size (number of lipids), and with various compositions, including mixtures. The simulation temperatures, system compositions and areas per lipid A_l are given in the Supporting Information. The different patch sizes serve for size-consistency analysis and the compositions were chosen so we could verify that our code also works for lipid mixtures. The results of our method for the MARTINI patches are given in Table 2. We find the expected order of rigidity for the single-component patches, except for the surprising result that DMPC is found to be less flexible than DPPC. Yet, this can be attributed to the higher temperature of the DPPC simulation. At the same ΔT to the Gel-to-liquid phase transition temperature, DMPC is in fact predicted to be more rigid [44]. The lipid mixtures do not express strong clear trends for moduli, except for a slight hardening with the addition of either cholesterol or PE. However, the effect of cholesterol is not very strong, at least at low mole fractions. This weak effect of cholesterol in the low concentration regime has already been observed and reported in [45]. O-Lyso-PC is not in fact stable as a bilayer, but only remains lamellar due to finite size effect. Nevertheless, its low bending modulus is in line with expectations [46]. We also simulated a larger patch of this lipid, where it spontaneously transitioned to a micellar phase (c.f. Table 3). To compare with the current implementation of the real-space fluctuation method [38] (ReGiS), we, furthermore, computed elastic moduli for a number of all-atom systems. In addition, we tested the response of these moduli to temperature and phase changes (see Supporting Information for Simulation Details). To dissect the thermodynamic components of entropy and enthalpy of tilt and bend, we used small patches of all-atom lipid models, scanned over temperature. (Details are also in the Supporting Information).

5.2. Comparing results of the different methods

5.2.1. ReSIS versus ReGiS

In Fig. 7, the results of ReSIS for the systems detailed in the Supporting Information are compared with the older real-space implementation (ReGiS) [38]. We find very good agreement of both κ and κ_θ for both methods. The most significant deviations are found for the POPE/POPG mixture. We recalculated the bending modulus for this lipid with the director fluctuation method, obtaining a values of $\kappa = 15.81\ k_BT$, almost exactly midway between the two values from ReGiS and ReSIS. Another outlier is POPC, where we find a higher value for the bending modulus derived by ReSIS compared to the ReGiS value. While both values are within the experimental margin of error, the ReSIS value is closer to the reported director fluctuation value of $\kappa = 15.8\ k_BT$ [35,34]. This indicates that the

real-space results are within the margin of uncertainty for the two different implementations.

5.2.2. ReSIS versus Fourier space methods

In Fig. 8 left panel, results from the ReSIS method are compared to results from the Fourier-space based director fluctuation method. We find good agreement, with bending moduli scattered above and below the Fourier based results. We checked for consistency of the Fourier space methods in Fig. 8 right panel. It should be noted that the height fluctuation methodology produces very large uncertainties, compared to the director fluctuation method – especially in the presence of cholesterol, resulting in an outlier in the Fourier spectrum that biases the fit. We find that in our implementation of the height fluctuation method, the spectrum contains several outliers (see also Fig. 1), which are not normally appreciably present in the low q regime, but do appear in the case of some cholesterol containing membranes. This might be caused by the relative vertical mobility of CHOL with respect to neighboring phospholipids. A similar observation was made previously, regarding the effect of CHOL position in the bilayer on the tilt modulus [47]. This is also reflected in the comparison of the director fluctuations with height fluctuations, (right panel of Fig. 8). The DOPC/DOPS/CHOL mixture is again an outlier. With these exceptions, the Fourier-space and ReSIS methods agree that the differences between mixtures are not very large. We also find a lower bending modulus for DOPE than derived in both director and height fluctuation method. In this context, recall that the real space methods derive a fundamentally different quantity from the Fourier fluctuation methods. Namely, in the real space analysis we compute a thermodynamic susceptibility, whereas the fluctuation methods extract the *model*-quantity as given in the Hamiltonian (see discussion in Section 4.4). These two quantities differ even in the mean field approach, as has been shown for the tilt modulus in [37,34]. In view of this, it is surprising to see how close these different quantities are when extracted using the two approaches.

Finally, in Fig. 9 we compare the ReSIS tilt moduli to the director-fluctuation tilt moduli. Only few data on MARTINI tilt moduli have been published for the director-fluctuation methodology. Our value for DPPC agrees with the one reported in the original implementation [15]. We find the moduli to be similar for the two methods. This is rather surprising, since mean-field theory predicts that in general the model-tilt modulus should be lower than the thermodynamic tilt ([37]), whereas we find the contrary. This highlights how little is known about the tilt modulus and the relation of Hamiltonian and susceptibility moduli in general. This phenomenon, however, seems to be restricted to MARTINI lipids, as the director fluctuation approach yields lower tilt moduli in

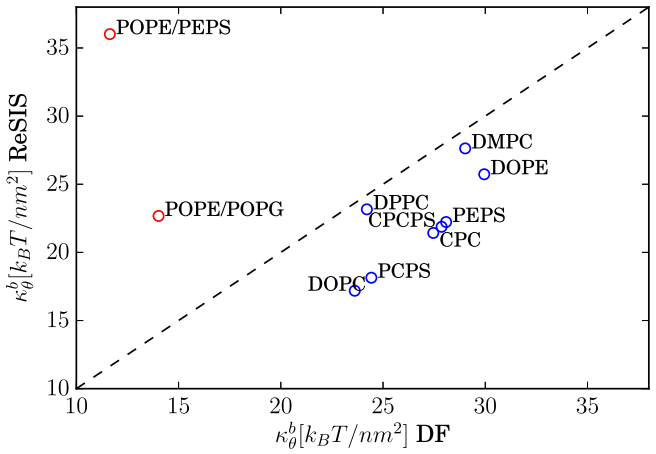

Fig. 9. Comparison of bilayer ReSIS tilt moduli with Fourier-space director fluctuation tilt moduli. Blue circles are from MARTINI simulations, red circles are from all-atom simulations. Abbreviations are defined in Table 2. (For interpretation of the references to colour in this figure legend, the reader is referred to the web version of this article.)

the case of all-atom simulations, as shown in red in the graphic. For a detailed comparison see [11]. We conclude the comparison by restating the very satisfactory agreement of the ReSIS method with the ReGiS method. The Fourier-based methods also agree well with each other.

Finally, for a detailed comparison, the results are summarized in the comparison Tables 1, and 2. Where values are missing, this is due to patch size being to too small to analyze, so that we could not find any semblance of the required convergence in the fluctuation. This is also a factor when considering tilt moduli values derived from the DF method, Table 1.

5.3. Lipids under nonstandard conditions

In order to test the universality and applicability of the ReSIS approach, we computed bending and tilt moduli at different temperatures, and for metastable states and highly curved nonlamellar phases. The results are shown in Fig. 10 and summarized in Table 3. As expected, the bending and tilt moduli increase as temperature decreases. This effect is especially strong in the case of DPPC, where 300 K is even lower than the experimental gel-to-liquid phase transition temperature. We note that the O-Lyso-PC bending modulus and DOPE bending moduli are lower in the nonlamellar phases compared with the flat bilayer. We find tilt moduli to be

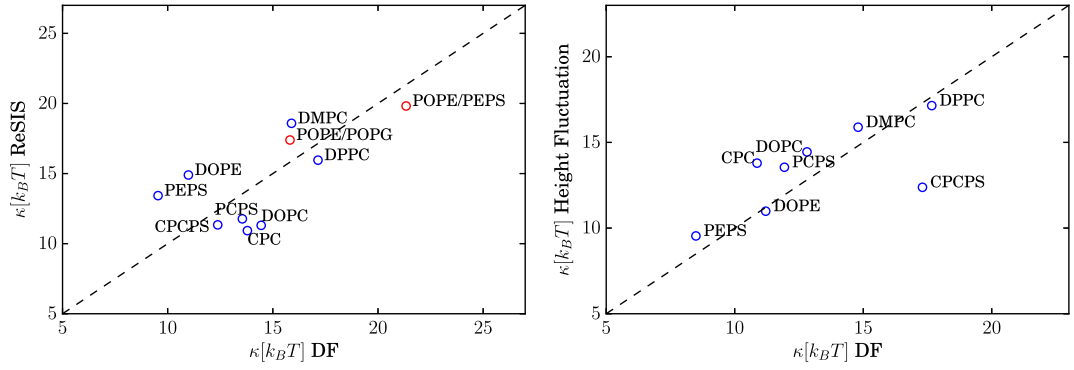

Fig. 8. Comparison of Fourier-based methods with each other and with the real-space implementation ReSIS Left panel: Comparison of the director fluctuation (DF) method with ReSIS. The red circles are derived from all-atom simulations. The blue circles are from MARTINI simulations. Right panel: Comparison of the height fluctuation method with the director fluctuation method. Abbreviations are defined in Table 2. (For interpretation of the references to colour in this figure legend, the reader is referred to the web version of this article.)

Table 1
Comparison of bending and tilt moduli for all-atom patches, ReGiS values taken from [11]. Monolayer bending moduli in k_BT and bilayer tilt moduli in k_BT nm^{-2}. Molar mixture ratios are given in the SI.

Composition	κ ReSIS	κ ReGiS	κ_θ^b ReSIS	κ_θ^b ReGiS	κ_θ^b DF
POPC	14.12	12.15	18.57	19.81	–
POPC/PSM	17.73	16.25	24.39	26.45	–
POPE/POPG	17.39	14.3	22.99	24.24	14.02
POPE/POPS	19.82	20.25	34.09	35.13	11.63
DPPC	17.23	17.05	23.92	24.33	–

Table 2
Comparison of bending and tilt-moduli for large lipid patches. Monolayer bending moduli in k_BT and bilayer tilt moduli in k_BT nm^{-2}. All-atom simulations are marked with *AA* in superscript. Abbreviations for mixtures are in brackets. Molar mixture ratios are given in the SI.

Composition	κ ReSIS	κ Height	κ DF	κ_θ^b ReSIS	$\kappa^b\theta$ DF
POPE/POPG^{AA}	17.39	–	15.81	23.00	14.02
POPE/POPS^{AA}	19.82	–	21.337	34.09	11.63
DOPE	14.89	11.2	10.98	25.73	29.94
DOPC	11.30	12.81	14.44	17.18	23.62
DPPC	15.95	17.66	17.14	23.16	24.20
DMPC	18.58	14.80	15.89	27.62	29.02
DOPC/DOPS (PCPS)	11.77	11.93	13.55	18.14	24.43
DOPE/DOPS (PEPS)	13.43	8.49	9.54	22.23	28.09
DOPC/DOPS/CHOL (CPCPS)	11.33	17.30	12.38	21.87	27.87
DOPC/CHOL (CPC)	10.92	10.86	13.79	21.42	27.46

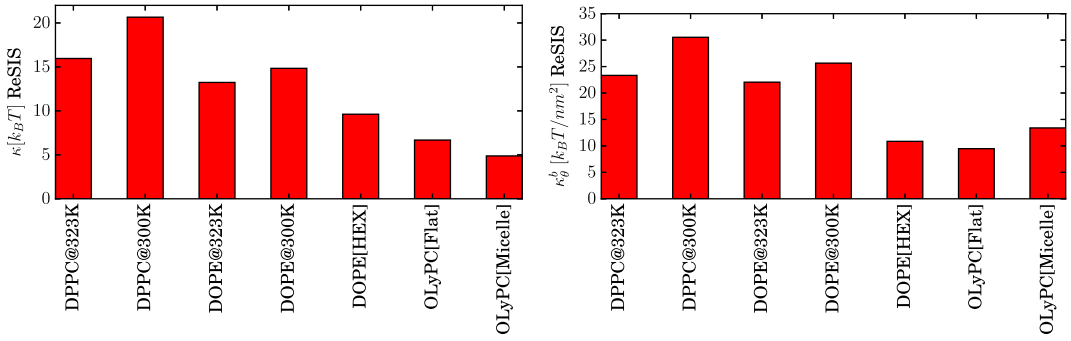

Fig. 10. Summary of results for MARTINI simulations. Left Panel: Monolayer bending moduli for lipids at different temperatures and in different phases, Right Panel: Bilayer tilt moduli for the same patches. OPC stands for O(leyl)-Lyso-PC, HEX for the inverted hexagonal phase.

Table 3
Bend and Tilt moduli for different phases and at different temperatures. Monolayer bending moduli in k_BT and bilayer tilt moduli in k_BT nm^{-2}.

Lipid	Condition	κ ReSIS	κ_θ^b ReSIS
DOPE	Inverted Hexagonal Phase	9.61	10.86
DOPE	Metastable Bilayer (968 Lipids)	14.81	25.6
O-Lyso-PC	Wormlike Micelle	4.87	13.40
O-Lyso-PC	Metastable Bilayer	6.68	9.47
DOPE	T = 323 K, 2048 Lipids	13.28	22.04
DPPC	T = 300 K, 2048 Lipids	20.66	30.54

strongly affected, with O-Lyso-PC exhibiting an increase in the positively curved phase. The lower DOPE tilt modulus found in the negatively curved phase agrees well with the results from ReGiS [16]. Values for the DOPE inverted hexagonal phase using ReGiS are κ = 8.0 k_BT [16] and κ_θ^b = 9.1. In the case of DOPE a slight mean spontaneous tilt divergence of $\langle \mathrm{Div}(\mathbf{t}) \rangle = 0.09$ nm^{-1} was apparent in the analysis. In this context it should be pointed out that there is absolutely no guarantee that the neutral plane is independent of mean curvature. Nevertheless, the offset did not strongly affect the resulting modulus as we also verified by using a different base for the instantaneous surface. In the case of O-LysoPC no adjustments had to be made as the tilt divergence distribution was still centered around 0. We used the bilayer A_l to compute the moduli, as was validated in [16]. These results demonstrate how curvature softening can be witnessed using ReSIS analysis. In addition, even micelle systems are in principle amenable to ReSIS. However, we acknowledge that further fine-tuning of the method may be necessary, especially for highly curved interfaces. A first step towards this in the future will be to implement an instantaneous area-per-lipid estimator. However, we believe the method is already highly useful even for qualitative analysis of rapidly deforming patches or phase transitions.

5.4. Temperature dependence of elastic moduli

Fig. 11 shows the value of the tilt and bending moduli for DPPC as a function of temperature (for details see Table 4 and the Supporting Information). The figure shows that as temperature rises, the moduli decrease monotonically. This change is consistent with the known general trend of membrane thinning with rising temperature, potentially leading to membrane softening seen as a decrease in membrane elastic moduli. To further dissect each of these moduli into their entropic and energetic (enthalpic) contributions, we performed a van 't Hoff analysis for the temperature dependence of the moduli. In order to change only the temperature as the relevant intensive variable, for the purpose of this analysis,

Table 4
Bend and Tilt moduli for saturated lipids. Constant pressure simulations Monolayer bending moduli in $10^{-20}J$ and monolayer tilt moduli in 10^{-20} J nm^{-2}, temperature in Kelvin. All patches have 64 lipids per leaflet.

Lipid	Temperature	κ_θ ReSIS	κ ReSIS
DMPC	303	10.41 ± 0.23	17.20 ± 0.20
DSPC	343	9.74 ± 0.21	16.63 ± 0.30
DPPC	320	10.67 ± 0.57	18.23 ± 0.49
DPPC	323	10.02 ± 0.25	16.92 ± 0.30
DPPC	326	9.43 ± 0.16	16.26 ± 0.13
DPPC	329	9.43 ± 0.16	16.33 ± 0.16
DPPC	332	9.19 ± 0.16	15.90 ± 0.27
DPPC	335	9.09 ± 0.11	15.57 ± 0.28
DPPC	338	8.84 ± 0.10	14.93 ± 0.20
DPPC	341	8.92 ± 0.10	14.86 ± 0.15
DPPC	344	8.72 ± 0.15	14.86 ± 0.17

temperature is varied while maintaining the area of the lipid patch (and thus the average area per lipid) constant at its equilibrium value at a reference temperature ($T_0 = 323$ K for DPPC). Fitting the resulting tilt moduli to the expression

$$\kappa_\theta(T) = H_0 + C_p(T - T_0) - T\left(S_0 + C_p \ln\frac{T}{T_0}\right) \tag{40}$$

and the bending moduli to a corresponding expression, we are able to extract the values of the entropy and enthalpy contributions to the two moduli. Fig. 11 shows the fits, and Table 5 gives the values of entropy and enthalpy at the reference temperature. Interestingly, the tilt modulus, and to lesser extent the bending modulus, rise in this constant-area ensemble, reflecting considerable entropic contributions. We find an entropic contribution that dominates the value of the tilt modulus. To contrast, enthalpy is lower (in absolute value) and favors tilt, counteracting to some extent the effect of entropy. The bending modulus is also dominated by an entropic contribution, but the enthalpic contribution is small. These trends can be seen also for other PC lipids with chains of different lengths, in Fig. 12 and Table 5.

These results indicate that both bend and tilt degrees of freedom behave as *entropic springs*, whereby tilting or bending away from the equilibrium state restricts the number of accessible states, thereby lowering entropy. This reduced entropy is the main driving force restricting bending deformations and limiting tilt to lower angles. This mechanism is analogous to the mechanism of polymer elasticity, where a stiffening is expected upon heating, and has been suggested as the underlying mechanism of membrane bending stiffness [26]. That enthalpy for tilting is favorable is, perhaps, surprising, and is likely due to better packing or lower conformational energy associated with tilted chains. This enthalpic contribution potentially heralds the emergence of spontaneous collective tilt of lipid chains when some lipids are cooled below the gel-to-liquid transition temperature. Finally, the values from the fitting procedure show a heat capacity C_p that is small or cannot be precisely determined from the fit; see Table 5 and values derived with heat capacity used as a fit parameter or constrained to a value of zero.

Table 5
Entropy and enthalpy of tilt and bending moduli, extracted from the van 't Hoff fit. Reported values are given in 10^{-20} J nm^{-2}.

Lipid	$T_0 - T_m$ [K]	Fit Range [K]	H_0	$-T_0S_0$	C_P
Tilt modulus					
DMPC	6	3–15	33.4 ± 34.9	23.7 ± 34.4	−9.6 ± 7.2
			−11.4 ± 11.8	21.0 ± 11.6	0 (fixed)
DPPC	9	6–30	−15.0 ± 5.1	24.7 ± 5.6	0.13 ± 0.53
			−13.7 ± 1.8	23.4 ± 1.6	0 (fixed)
DSPC	15	9–21	−19.1 ± 2.3	28.9 ± 1.5	−2.0 ± 0.9
			−18.9 ± 1.5	28.7 ± 2.3	0 (fixed)
Bending modulus					
DMPC	6	3–15	−0.32 ± 18.65	17.1 ± 18.6	1.1 ± 3.9
			4.7 ± 3.75	12.1 ± 3.7	0 (fixed)
DPPC	9	6–30	−1.4 ± 6.8	18.1 ± 6.7	−0.29 ± 0.6
			−4.6 ± 1.9	21.3 ± 1.8	0 (fixed)
DSPC	15	9–21	−2.8 ± 4.2	18.2 ± 4.4	−2.3 ± 2.5
			−1.8 ± 4.4	19.3 ± 4.1	0 (fixed)

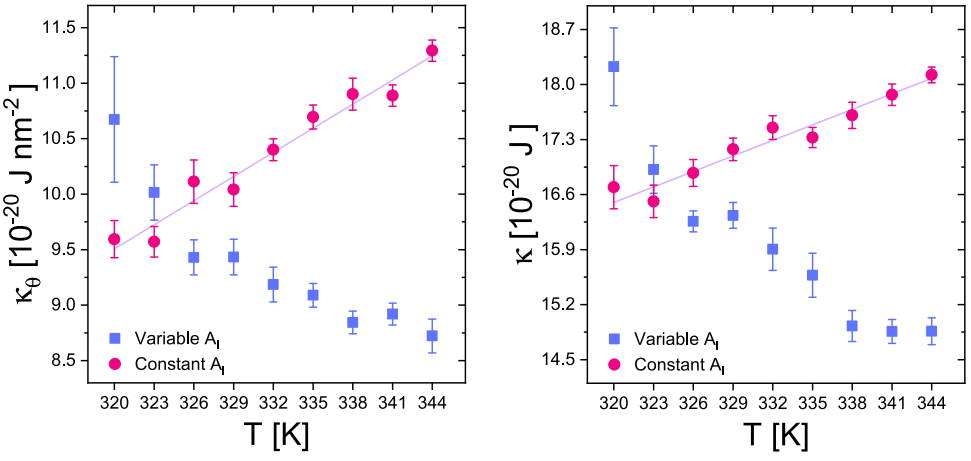

Fig. 11. Temperature dependence of tilt (left) and bending (right) moduli of DPPC taken two ways: at constant pressure, and at constant area per lipid. Lines show fits to Eq. (40).

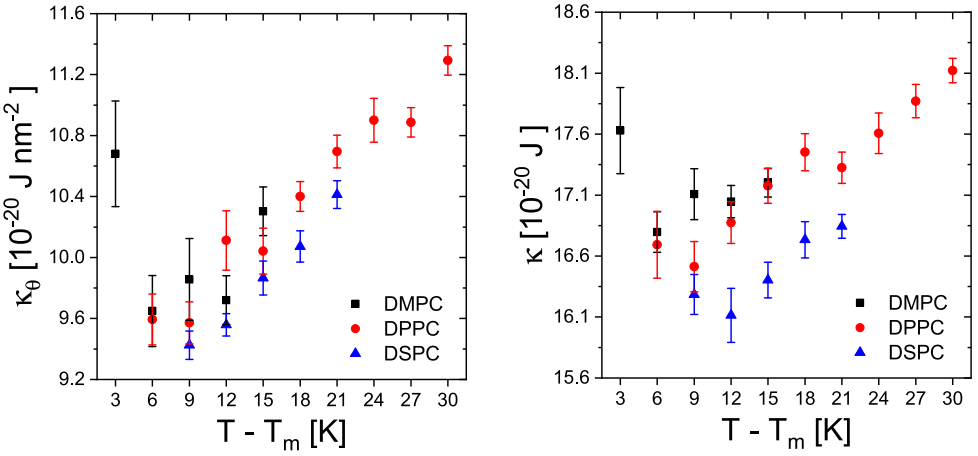

Fig. 12. Temperature dependence of tilt (left) and bending (right) moduli of DSPC, DPPC, and DMPC using a constant surface area ensemble, showing similar slope for different lipids. This reflects a similar decomposition into enthalpic and entropic contributions to the moduli. Temperature is reported as a distance to the main gel-to-lipid transition temperature.

5.5. Dependence on the software and hardware

Many properties of lipid bilayers are susceptible to algorithmic or even implementation details found in different available molecular dynamics software [48,49]. For example, we find the DPPC κ using NAMD [50]to be 17.2 kT, whereas the GROMACS 5 [51]result for the same temperature is 18.9 kT. The corresponding tilt moduli κ_θ^b values of 22.5 kT and 23.9 kT are somewhat closer. In the SI we give DMPC results for different GROMACS 5 versions and hardware. All trajectories were generated from the same topology. We find differences of up to 1.5 kT for κ and κ_θ^b, despite using a fixed area ensemble. These differences are apparently nonsystematic; however, we strongly recommend to use the same computational setup and implementation when comparing bending moduli of different lipids. Furthermore, we found the largest differences between implementations close to T_m, the gel-to-liquid transition temperature, so careful equilibration is necessary in that vicinity.

6. Computational details

The simulations used to validate the instantaneous tilt field method were taken from previous studies, and computational details may be found there [11,16]. New simulations used GROMACS. Specifically, GROMACS 5.0.4 was used for all-atom simulations, and GROMACS 5.1.4 was used for coarse-grained (CG) simulations, unless stated otherwise. The coarse-grained simulations used the MARTINI forcefield and all-atom simulations used the CHARMM36 [52] forcefield for lipids and the CHARMM-TIP3P [53] model for water. For the coarse grained MD, we use reaction-field electrostatics with an ε_r of 15. All-atom simulations used Particle-Mesh-Ewald electrostatics [54]. Simulations were run in an NpT ensemble. We used a CSVR [55] thermostat with a coupling constant of 1 ps and the Parrinello-Rahman barostat [56] configured for semiisotropic pressure coupling at 1 bar with a coupling constant of 12 ps. The MARTINI nonbonded cutoff was 1.1 nm, and the timestep was 30 fs. All CG-simulations were run for at least 1 μs, after undergoing some pre-equilibration. All-atom simulations were run for 200 ns at CHARMM-GUI [57] default settings. The first 50 ns were used for equilibration. For the initial construction of the MARTINI patches and topology we used *insane* [58], for the construction of the all-atom topologies we used CHARMM-GUI.

7. Conclusion

We have summarized existing strategies for obtaining membrane elastic moduli and clarified the differences in the underlying concepts. Our analysis also highlighted how these strategies may be improved upon. This has led us to propose a new spatially local method for extracting the bending and tilt moduli, based on an instantaneous estimation of the membrane surface. We have shown the method's insensitivity to the simulated membrane patch size, and have applied it to a large variety of systems, including mixtures and curved membrane geometries. In addition, we have provided alternative implementations of various available Fourier-space methods. Comparing the results of these methods with each other and to published data, we found good agreement between Fourier analysis based methods, as well as between real space-based ones. We discuss the differences between the *thermodynamic* real space- and *model* Hamiltonian Fourier based moduli. We specifically focus on the tilt modulus, where significant differences between Fourier and real-space methods are observed. We also re-examined the angular degeneracy of the tilt vector and its effect on the probability density. Finally, a van 't Hoff analysis of the tilt and bending moduli reveals that both modes act as entropic springs and that, perhaps surprisingly, enthalpy favors nonzero tilt.

Acknowledgement

We thank Milka Doktorova and George Khelashvili for helpful ongoing discussions and for making available their simulation trajectories. CA thanks the Minerva Foundation for a postdoctoral fellowship. The Fritz Haber Research Center is supported by the Minerva Foundation, Munich, Germany.

Appendix A. Supplementary data

The implementations used for this study are made available on the Harries group website https://scholars.huji.ac.il/danielharries/lipidator-toolkit, and on GitHub (https://github.com/allolio/lipidator-toolkit). There we also make available a set of director definitions compatible with [11], surface atom definitions and a manual on how to use the software.

The Supporting Information contains further simulation details, bending moduli for fixed area simulations and results for different

computational setups as well as implementation details for the software used in this paper. Supplementary data associated with this article can be found, in the online version, at https://doi.org/10.1016/j.chemphys.2018.03.004.

References

[1] W. Helfrich, Elastic properties of lipid bilayers: theory and possible experiments, Z. Naturforsch. C 28 (1973) 693–793.
[2] Y. Schweitzer, T. Shemesh, M. Kozlov, A model for shaping membrane sheets by protein scaffolds, Biophys. J. 109 (3) (2015) 564–573.
[3] L.V. Chernomordik, M.M. Kozlov, Mechanics of membrane fusion, Nat. Struct. Mol. Biol. 15 (2008) 675–683.
[4] S.A. Safran, Statistical Thermodynamics of Surfaces, Interfaces, and Membranes, Westview Press, Boulder Colorado, 2003.
[5] C. Nielsen, M. Goulian, O.S. Andersen, Energetics of inclusion-induced bilayer deformations, Biophys. J. 74 (4) (1998) 1966–1983.
[6] L. Vamparys, R. Gautier, S. Vanni, W.D. Bennett, D.P. Tieleman, B. Antonny, C. Etchebest, P. Fuchs, Conical lipids in flat bilayers induce packing defects similar to that induced by positive curvature, Biophys. J. 104 (3) (2013) 585–593.
[7] R. Mukhophadhyay, H.W.G. Lim, M. Wortis, Echinocyte shapes: bending, stretching, and shear determine spicule shape and spacing, Biophys. J. 82 (2002).
[8] J. Agudo-Canalejo, R. Lipowsky, Uniform and janus-like nanoparticles in contact with vesicles: energy landscapes and curvature-induced forces, Soft Matter 13 (2017) 2155–2173.
[9] Y. Kozlovsky, A. Efrat, D.A. Siegel, M.M. Kozlov, Stalk phase formation: effects of dehydration and saddle splay modulus, Biophys. J. 87 (4) (2004) 2508–2521.
[10] R. Dimova, Recent developments in the field of bending rigidity measurements on membranes, Adv. Colloid Interface Sci. 208 (2014) 225–234.
[11] M. Doktorova, D. Harries, G. Khelashvili, Determination of bending rigidity and tilt modulus of lipid membranes from real-space fluctuation analysis of molecular dynamics simulations, Phys. Chem. Chem. Phys. 19 (2017) 16806–16818.
[12] J.F. Nagle, M.S. Jablin, S. Tristram-Nagle, Sugar does not affect the bending and tilt moduli of simple lipid bilayers, Chem. Phys. Lipids 196 (Suppl. C) (2016) 76–80.
[13] C. Allolio, K. Baxova, M. Vazdar, P. Jungwirth, Guanidinium pairing facilitates membrane translocation, J. Phys. Chem. B 120 (1) (2016) 143–153.
[14] A. Magarkar, P. Jurkiewicz, C. Allolio, M. Hof, P. Jungwirth, Increased binding of calcium ions at positively curved phospholipid membranes, J. Phys. Chem. Lett. 8 (2) (2017) 518–523.
[15] M.C. Watson, E.G. Brandt, P.M. Welch, F.L.H. Brown, Determining biomembrane bending rigidities from simulations of modest size, Phys. Rev. Lett. 109 (2012) 028102.
[16] N. Johner, D. Harries, G. Khelashvili, Curvature and lipid packing modulate the elastic properties of lipid assemblies: comparing H_{II} and lamellar phases, J. Phys. Chem. Lett. 5 (23) (2014) 4201–4206.
[17] M.M. Terzi, M. Deserno, Novel tilt-curvature coupling in lipid membranes, J. Chem. Phys. 147 (8) (2017) 084702.
[18] G. Khelashvili, B. Kollmitzer, P. Heftberger, G. Pabst, D. Harries, Calculating the bending modulus for multicomponent lipid membranes in different thermodynamic phases, J. Chem. Theory Comput. 9 (9) (2013) 3866–3871.
[19] V.A. Harmandaris, M. Deserno, A novel method for measuring the bending rigidity of model lipid membranes by simulating tethers, J. Chem. Phys. 125 (20) (2006) 204905.
[20] E.R. May, A. Narang, D.I. Kopelevich, Molecular modeling of key elastic properties for inhomogeneous lipid bilayers, Mol. Simul. 33 (9–10) (2007) 787–797.
[21] B. Kollmitzer, P. Heftberger, R. Podgornik, J. Nagle, G. Pabst, Bending rigidities and interdomain forces in membranes with coexisting lipid domains, Biophys. J. 108 (12) (2015) 2833–2842.
[22] A. Sodt, R. Pastor, Bending free energy from simulation: correspondence of planar and inverse hexagonal lipid phases, Biophys. J. 104 (10) (2013) 2202–2211.
[23] P. Canham, The minimum energy of bending as a possible explanation of the biconcave shape of the human red blood cell, J. Theor. Biol. 26 (1) (1970) 61–81.
[24] E. Evans, Bending resistance and chemically induced moments in membrane bilayers, Biophys. J. 14 (12) (1974) 923–931.
[25] I. Szleifer, D. Kramer, A. Ben-Shaul, W.M. Gelbart, S.A. Safran, Molecular theory of curvature elasticity in surfactant films, J. Chem. Phys. 92 (11) (1990) 6800–6817.
[26] A. Ben-Shaul, W. Gelbart, Statistical thermodynamics of amphiphile self-assembly: structure and phase transitions in micellar solutions, in: Gelbart, Ben Shaul, Roux (Eds.), Micelles, Membranes, Microemulsions and Monolayers, Springer-Verlag, New York Inc, New York, 1994, pp. 1–104.
[27] P. Diggins, Z.A. McDargh, M. Deserno, Curvature softening and negative compressibility of gel-phase lipid membranes, J. Am. Chem. Soc. 137 (40) (2015) 12752–12755.
[28] F.C. Frank, I. liquid crystals. On the theory of liquid crystals, Discuss. Faraday Soc. 25 (1958) 19–28.
[29] Y. Kozlovsky, M.M. Kozlov, Stalk model of membrane fusion: solution of energy crisis, Biophys. J. 82 (2) (2002) 882–895.
[30] M. Hamm, M. Kozlov, Elastic energy of tilt and bending of fluid membranes, Eur. Phys. J. E 3 (4) (2000) 323–335.
[31] R. Goetz, G. Gompper, R. Lipowsky, Mobility and elasticity of self-assembled membranes, Phys. Rev. Lett. 82 (1999) 221–224.
[32] S.J. Marrink, A.H. de Vries, A.E. Mark, Coarse grained model for semiquantitative lipid simulations, J. Phys. Chem. B 108 (2) (2004) 750–760.
[33] S.J. Marrink, D.P. Tieleman, Perspective on the martini model, Chem. Soc. Rev. 42 (2013) 6801–6822, 10.1039/C3CS60093A.
[34] J.F. Nagle, Experimentally determined tilt and bending moduli of single-component lipid bilayers, Chem. Phys. Lipids 205 (2017) 18–24.
[35] Z.A. Levine, R.M. Venable, M.C. Watson, M.G. Lerner, J.-E. Shea, R.W. Pastor, F.L. H. Brown, Determination of biomembrane bending moduli in fully atomistic simulations, J. Am. Chem. Soc. 136 (39) (2014) 13582–13585.
[36] P. Diggins, M. Deserno, Determining the bending modulus of a lipid membrane by simulating buckling, J. Chem. Phys. 138 (21) (2013) 214110.
[37] S. May, Y. Kozlovsky, A. Ben-Shaul, M. Kozlov, Tilt modulus of a lipid monolayer, Eur. Phys. J. E Soft Matter 14 (3) (2004) 299–308.
[38] N. Johner, D. Harries, G. Khelashvili, Implementation of a methodology for determining elastic properties of lipid assemblies from molecular dynamics simulations, BMC Bioinf. 17 (1) (2016) 161.
[39] S.J. Marrink, A.E. Mark, Effect of undulations on surface tension in simulated bilayers, J. Phys. Chem. B 105 (26) (2001) 6122–6127.
[40] J.M. Vanegas, A. Torres-Snchez, M. Arroyo, Importance of force decomposition for local stress calculations in biomembrane molecular simulations, J. Chem. Theory Comput. 10 (2) (2014) 691–702.
[41] M. Berger, A. Tagliasacchi, L. Seversky, P. Alliez, J. Levine, et al., State of the art in surface reconstruction from point clouds, Eurogr. Star Rep. 1 (2014) 161–185.
[42] R.J. Baxter, Exactly Solved Models in Statistical Mechanics, Dover Publications Inc., 2008.
[43] J.F. Nagle, X-ray scattering reveals molecular tilt is an order parameter for the main phase transition in a model biomembrane, Phys. Rev. E 96 (2017) 030401.
[44] A.C. Woodka, P.D. Butler, L. Porcar, B. Farago, M. Nagao, Lipid bilayers and membrane dynamics: Insight into thickness fluctuations, Phys. Rev. Lett. 109 (2012) 058102.
[45] G. Khelashvili, M. Rappolt, S.-W. Chiu, G. Pabst, D. Harries, Impact of sterol tilt on membrane bending rigidity in cholesterol and 7dhc-containing dmpc membranes, Soft Matter 7 (2011) 10299–10312.
[46] J.R. Henriksen, T.L. Andresen, L.N. Feldborg, L. Duelund, J.H. Ipsen, Understanding detergent effects on lipid membranes: a model study of lysolipids, Biophys. J. 98 (10) (2010) 2199–2205.
[47] G. Khelashvili, G. Pabst, D. Harries, Cholesterol orientation and tilt modulus in DMPC bilayers, J. Phys. Chem. B 114 (22) (2010) 7524–7534.
[48] S. Reier, D. Poger, M. Stroet, A.E. Mark, Real cost of speed: the effect of a time-saving multiple-time-stepping algorithm on the accuracy of molecular dynamics simulations, J. Chem. Theory Comput. 13 (6) (2017) 2367–2372.
[49] J. Lee, X. Cheng, J.M. Swails, M.S. Yeom, P.K. Eastman, J.A. Lemkul, S. Wei, J. Buckner, J.C. Jeong, Y. Qi, S. Jo, V.S. Pande, D.A. Case, C.L. Brooks, A.D. MacKerell, J.B. Klauda, W. Im, Charmm-gui input generator for namd, gromacs, amber, openmm, and charmm/openmm simulations using the charmm36 additive force field, J. Chem. Theory Comput. 12 (1) (2016) 405–413.
[50] J.C. Phillips, R. Braun, W. Wang, J. Gumbart, E. Tajkhorshid, E. Villa, C. Chipot, R. D. Skeel, L. Kalé, K. Schulten, Scalable molecular dynamics with namd, J. Comp. Chem. 26 (16) (2005) 1781–1802.
[51] M.J. Abraham, T. Murtola, R. Schulz, S. Páll, J.C. Smith, B. Hess, E. Lindahl, Gromacs: high performance molecular simulations through multi-level parallelism from laptops to supercomputers, SoftwareX 12 (2015) 19–25.
[52] R.B. Best, X. Zhu, J. Shim, P.E.M. Lopes, J. Mittal, M. Feig, J. Alexander, D. MacKerell, Optimization of the additive charmm all-atom protein force field targeting improved sampling of the backbone ϕ, ψ and side-chain χ^1 and χ^2 dihedral angles, J. Chem. Theory Comput. 8 (9) (2012) 3257–3273.
[53] W.L. Jorgensen, J. Chandrasekhar, J.D. Madura, R.W. Impey, M.L. Klein, Comparison of simple potential functions for simulating liquid water, J. Chem. Phys. 79 (1983) 926–935.
[54] U. Essman, L. Perela, M.L. Berkowitz, T. Darden, H. Lee, L.G. Pedersen, A smooth particle mesh ewald method, J. Chem. Phys. 103 (1995) 8577–8593.
[55] G. Bussi, D. Donadio, M. Parrinello, Canonical sampling through velocity rescaling, J. Chem. Phys. 126 (1) (2007) 014101.
[56] M. Parrinello, A. Rahman, Crystal structure and pair potentials: a molecular-dynamics study, Phys. Rev. Lett. 45 (1980) 1196.
[57] S. Jo, T. Kim, V.G. Iyer, W. Im, Charmm-gui: a web-based graphical user interface for charmm, J. Comp. Chem. 29 (11) (2008) 1859–1865.
[58] T.A. Wassenaar, H.I. Inglfsson, R.A. Backmann, D.P. Tieleman, S.J. Marrink, Computational lipidomics with insane: a versatile tool for generating custom membranes for molecular simulations, J. Chem. Theory Comput. 11 (5) (2015) 2144–2155.